Build Simul (2022) 15: 1309–1321
https://doi.org/10.1007/s12273-021-0856-x

Thermal environment investigation of asymmetric radiation coupled with convection heating

Man Fan[1,2,3], Jia Wang[1], Lanlan Zhang[1], Han Li[1], Xiangfei Kong[1] (✉), Chenxiao Zheng[4]

1. School of Energy and Environmental Engineering, Hebei University of Technology, Tianjin 300401, China
2. State Key Laboratory of Building Safety and Built Environment, Beijing 100013, China
3. National Engineering Research Center of Building Technology, Beijing 100013, China
4. School of Mechanical Engineering, Tianjin University of Commerce, Tianjin 300134, China

Abstract

The couple of radiation with convection heating owned advantages of less energy utilization, healthier and more comfortable indoor environment. However, local thermal discomfort was often induced by large vertical temperature difference and radiation asymmetry temperature. This work studied indoor thermal environment characteristics under different coupling ways of radiation and convection heating terminals through experiments and CFD simulation. The studied five scenarios were denoted as: (I) lateral air supply + adjacent side wall radiation, (II) lateral air supply + opposite side wall radiation, (III) lateral air supply + floor radiation, (IV) lateral air supply + adjacent side wall radiation + floor radiation, and (V) lateral air supply + opposite side wall radiation + floor radiation. The overall thermal comfort indices (including air diffusion performance index (ADPI), predicted mean vote (PMV), and predicted percent of dissatisfaction (PPD)) and local thermal comfort indices under different scenarios were investigated. For Scenarios I–III, the local dissatisfaction rates caused by vertical air temperature difference were 0.4%, 0.1%, and 0.2%, respectively, which belonged to "A" class according to the ISO-7730 Standard. While the vertical asymmetric radiation temperature of Scenario I/II was about 6.5 °C lower than that of Scenario III/IV/V. The ADPI for Scenarios III–V were about respectively 5.7%, 16.7%, and 21.0% higher than that of Scenarios I–II, indicating that a large radiation area and radiation angle coefficient could reduce the discomfort caused by radiant temperature asymmetry. The coupling mode improved local discomfort by decreasing vertical temperature difference and radiation asymmetry temperature wherefore improving the PMV from −1.6 to −1. The lateral air supply coupled with asymmetric radiation heating could potentially improve the thermal comfort of occupied area, while the comprehensive effect of thermal environmental improvement, energy-saving, and cost-effectiveness needes to be further investigated.

Keywords

asymmetric radiation;
lateral air supply;
overall thermal comfort;
local thermal comfort;
CFD simulation

Article History

Received: 15 July 2021
Revised: 27 September 2021
Accepted: 18 October 2021

1 Introduction

Since December 2019, Corona virus disease 2019 (COVID-19) spread rapidly all over the world within a short period, and a growing number of cases have proven the possibility of airborne transmission. Ensuring an adequate ventilation rate exerted to be an essential method to reduce the risk of infection in confined spaces (Dai and Zhao 2020; Xu et al. 2020), as it could reduce exposure risk of susceptible people by diluting pathogen concentration (Qian et al. 2021; Wang et al. 2021). ASHRAE (2020) suggested to strengthen the use of natural and mechanical ventilation in epidemic prevention, including dilution ventilation, personalized ventilation, directional ventilation, source capture ventilation, local exhaust, differential pressure ventilation, and so on. Actually, natural ventilation was usually difficult to be controlled, which led to non-ignorable heat losses and poor air distributions, exerting great impact on human health,

E-mail: xfkong@hebut.edu.cn

List of symbols

c	specific heat capacity of air (J/(kg·°C))	t_j	temperature of j plane (°C)
F_j	angle coefficient of human body to j plane	t_{mrt}	average radiation temperature (°C)
F_N	angle coefficient of the N^{th} surface to the micro element	t_n	average indoor air temperature (°C)
I	heating film current (A)	t_N	temperature of N^{th} surface (°C)
m	air mass flow (kg/s)	t_p	average temperature of floor surface (°C)
N	number of wind speed measuring points	t_{pr}	plane radiation temperature (°C)
Q_h	heating supply (W)	Δt_{pr}	asymmetric radiation temperature (°C)
t_a	heating film temperature (°C)	Tu	turbulence intensity
$\Delta t_{a,y}$	vertical temperature difference of 0.1 m (ankle) and 1.1 m (head) (°C)	U	heating film voltage (V)
		u_i	monitoring point velocity (m/s)
t_i	monitoring point temperature (°C)	v	average wind speed (m/s)

comfort, and productivity (Ji et al. 2021; Zhao et al. 2021). Mechanical ventilation usually used a ventilator to introduce fresh air to the room, and the air amount, ventilation timelines and, air path could be effectively controlled without relying on external natural conditions (Zhu et al. 2021; Sui et al. 2021). Therefore, the mechanical ventilation played a significant role to remove indoor pollutants and maintain indoor air cleanliness, especially in northern winter when the outdoor temperature was low, and the haze was serious.

On the other hand, heating was also greatly needed in northern winter for the harsh outdoor weather conditions. In 2018, the heating energy consumption in the north of China accounted for about 26% of the total energy consumption by building operation (Energy Conservation Research Center of Tsinghua University 2020). There were various forms of heating terminals, which could be categorized into radiation and convection ones. Specifically, the fan coil, skirting line heating, radiant roof, and radiant floor were commonly used. Owing to the variety of heat source type, intensity, and location, the indoor temperature distribution possesses obvious non-uniform characters (Ren and Cao 2021). For example, Atienza Márquez et al. (2017) found that the indoor comfort controlled by fan coil was worse than that by radiant floor. Raising the temperature set point could increase the comfort level close to the floor heating system, while the energy consumption increased by 17.3%. In the skirting line heating system, the cold outdoor airflow was inhaled to the baseboard radiator, pre-heated in the narrow horizontal baseboard channel, and then the warm airflow exited throughout the slot opening to prevent the invasion of cold air into the room. Under this heating mode, temperature changes along the room length and height direction were both less than 1.5 °C (Ploskić and Holmberg 2011). Conceição and Lúcio (2011) found that the thermal comfort of floor radiation was better than that of roof radiation, while the combination of floor or roof radiation with side wall radiation could achieve better thermal comfort. Rhee and Kim (2015) comprehensively reviewed the effect of combined system, radiation temperature, people's habits in different regions on thermal comfort, and found that the radiation asymmetry caused by different spatial positions of radiation surfaces was the main factor. Seyam et al. (2014) drew a conclusion that the average indoor air temperature increased by 1.83 °C when the radiant ceiling area increased from 31.68 to 44.64 m^2. Besides, the radiation heating also had some disadvantages, such as large heat transfer area, slow dynamic response as well as poor air quality, which limited its popularization and application (Bäckström et al. 2015). Hence, to create a comfortable radiant thermal environment, suitable laying positions, and sizes of radiation heating terminals needed to be carefully designed.

In the past few years, there were increasing requirements for buildings to be both comfortable and energy efficient (Zhang et al. 2021). The coupling of radiation and convection stood out to be a promising solution, as it could improve the heat transfer rate, indoor temperature distribution, and air quality simultaneously. Specifically, under the heating system of radiation coupled with displacement ventilation, a lower vertical air temperature difference was obtained. The temperature at the head level was merely 1 °C higher over the feet level. The radiation combined with floor air supply system could significantly improve thermal comfort especially at the working area, as predicted mean vote (PMV) values were within the range of ±1.0 (Schiavon et al. 2015; Liu et al. 2019). The radiant and convective heat transfer coefficient of a light-weight overhead floor radiant heating system could increase to 4.2 and 3.9 W/(m^2·K), respectively, leading to the total heat transfer amount higher than that of traditional heating (Zhang et al. 2013). The response speed of a wall radiant panel combined with an air source heat pump system was demonstrated to be fast (Zhang et al. 2018). When the outdoor temperature was 4.0 °C, the system coefficient of performance (COP) was 3.11 (Dong et al. 2018). Besides, Wang et al. (2017) proposed a convective

overhead floor radiant heating system with heat exchange holes. Owning to the effect of natural convection, when the air flowed outward through heat exchange holes with the average speed of 0.1 m/s, the response speed of the system increased, and the average indoor temperature was 2.6 °C higher than that without heat exchange holes.

Previous studies showed that the coupled convection with radiant heating could improve the overall thermal comfort of occupants, while the local thermal discomfort induced by vertical temperature difference and radiation asymmetry temperature needed to be further investigated. Different combination modes and locations of radiation and convection heating terminals significantly affected the temperature and airflow distributions in the room. Therefore, this study mainly focused on the influence of different terminal laying positions and sizes in the case of asymmetric radiation coupled with convection heating. The thermal environment characteristics were numerically modeled and validated with experiments. The overall and local thermal comfort were subsequently compared and improved. Suggestions were made for identifying the most suitable heating terminal and hence providing a reference for the optimal design and control of the indoor environment.

2 Experimental method

2.1 Experimental laboratory

The heating experiment was conducted in a typical cold climate region of Tianjin, China. The three-dimensional size of the environmental cabin was 6 m (length) × 5.92 m (width) × 2.6 m (height), and its layout is presented in Figure 1. The heating supply system could be divided into two sub-systems, i.e., convection and radiation sub-systems.

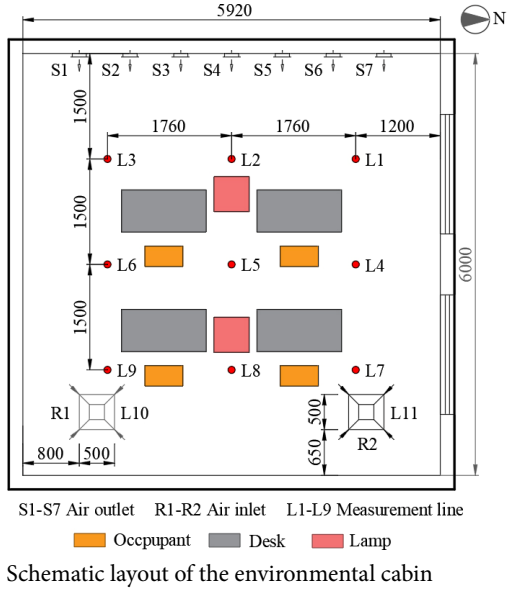

Fig. 1 Schematic layout of the environmental cabin

The convection sub-system used lateral air supply to directly send warm air to the personnel breathing area, and the radiation sub-system adopted electric radiant heating panels (ERHPs) as heat sources for side wall and floor heating. Details of these two sub-systems were presented in the following.

2.1.1 *Ventilation heating sub-system*

The test diagram of lateral air supply system is shown in Figure 2. The warm air was supplied from the square double deflection grille outlets (0.2 m × 0.2 m) located at 1.2 m in height (named as S1–S7) and returned through two air inlets (0.5 m × 0.5 m) on the ceiling (named as R1–R2). As a result, the warm air was directly sent to the personnel breathing area. This convection heating supply mode had higher thermal comfort and energy-saving level, and it was effective in removing indoor pollutants exhaled by occupants (Lin et al. 2012; Zhang et al. 2019).

2.1.2 *Radiation heating sub-system*

The diagram of radiation sub-system is depicted in Figure 3. The heating area of heating film on the side wall and floor were 7.8 and 35.5 m^2, respectively. By adjusting the input

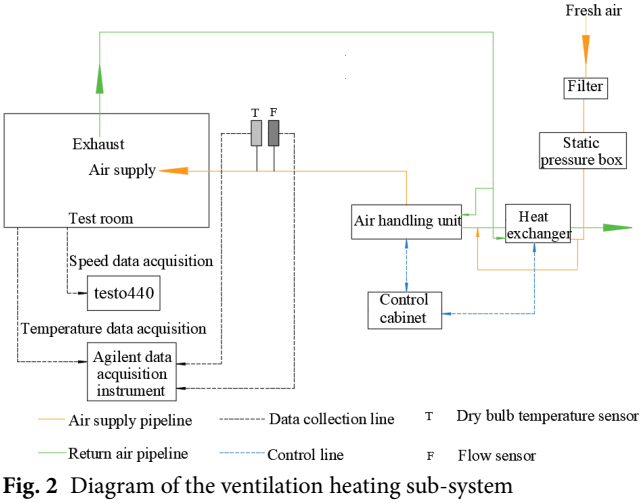

Fig. 2 Diagram of the ventilation heating sub-system

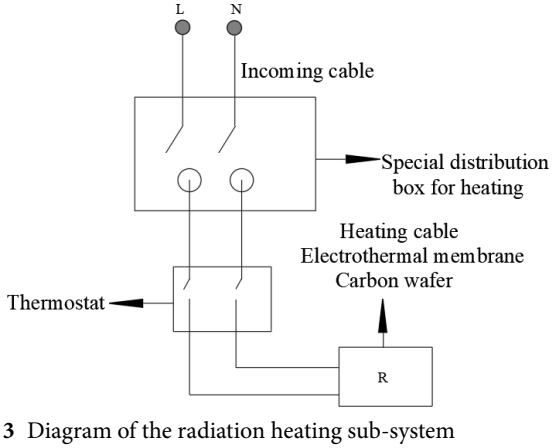

Fig. 3 Diagram of the radiation heating sub-system

voltage, the heating supply varied between 0–612 W and 0–2308 W, respectively. The floor radiant heating terminal comprised the cement particleboard (3 mm), the thermal insulation layer (3 mm), an electric radiant heating plate, and wooden floor and carpet (3 mm). The structure and photograph of the radiant heating terminals are depicted in Figure 4. The lateral ventilation, radiant side wall and floor heating could be used individually or in combination to control the indoor thermal environment.

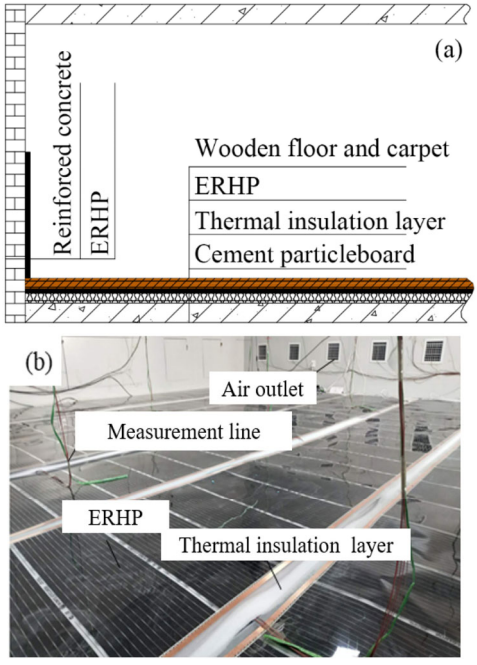

Fig. 4 (a) Structure and (b) photograph of the radiant heating terminals

2.2 Measuring devices

As depicted in Figure 1, 9 temperature measurement points at a height of 0.7 m were set for horizontal comparison. Moreover, 11 temperature measurement points at L5 measurement line with the height of 0.1, 0.3, 0.5, 0.7, 0.9, 1.1, 1.3, 1.5, 1.7, 1.9, and 2.4 m were set for vertical comparison. Therefore, a total of 19 measurement points were set for measuring the indoor air temperature. One Testo 480 hot-wire anemometer was used to measure and adjust the outlet air velocity accordingly. In addition, TH20R temperature and humidity recorder and Testo 440 black bulb thermometer were located at the height of 1.3 m in the center of the room. Data were recorded every 2 seconds and displayed in real time during the experiment. The ranges and accuracies of main measuring devices are provided in Table 1. The tested total heat supplied to the experimental laboratory was 3.55 kW, and its maximum error was 1.5%, which was regarded as acceptable by referring to Hu (2015).

Table 1 main measuring devices in the experiment

Measuring device	Type	Number	Range (accuracy)
T-type thermocouple	TT-T-30-SLE	19	−120 to 150 °C (±0.5 °C)
Hot wire anemometer	Testo 480	1	0 to 20 m/s (±0.05 m/s)
Temperature and humidity recorder	TH20R	1	−20 to 70 °C (±0.2 °C)
Black ball temperature	Testo 440	1	−200 to 1370 °C (±0.3 °C)

3 Numerical simulation

3.1 Numerical set-up

Airpak 3.0 software was used in this study owing to its powerful and extensive simulation capacity in the indoor environment (Fang et al. 2011). The physical model of the environmental cabin with desks, occupants, and lamps was built up according to its actual size, as shown in Figure 5. The standard k–ε model and discrete ordinate (DO) model were selected for their wide application range and reasonable precision. The convergence accuracy for continuity and momentum equation was set as 10^{-3}, while that for the energy equation was set as 10^{-6}. The first-order upwind scheme was selected for turbulent kinetic energy and turbulent dissipation rate, and the second-order upwind scheme was selected for the pressure, temperature, and momentum. The single-precision solver and default relaxation factor were selected by referring to Alonso et al. (2011). The occupants and lights were defined as solid boundary conditions, and their heat flux were set as 100 and 75 W, respectively (Kong et al. 2020). The roof, floor, and walls were modeled by utilizing the third kind of boundary conditions as shown in Table 2 (Camci et al. 2021).

As presented in Figure 6, three heating modes were modeled, namely lateral air supply, floor radiant heating,

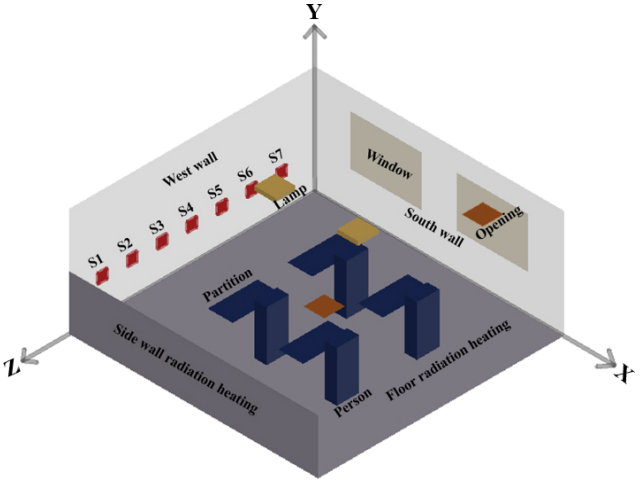

Fig. 5 Physical model of experimental cabin

Table 2 Boundary conditions of building envelope

Wall	Outdoor or adjacent room temperature (°C)	Heat transfer coefficient (W/(K·m²))
West wall	−11.6	2.19
East wall	−9.6	0.81
North Wall	−11.6	2.19
South wall	−9.6	0.81
Windows	−11.6	5.07
Floor	−7.6	0.81
Ceiling	−7.6	0.81

and side wall radiant heating. The radiation and convection heating parameters are provided in Table 3. Taking Scenario I as a reference case, Scenarios (I, III, IV) and (I, II, IV, V) were selected to investigate the influence of different combined heating modes (radiation and convection) and terminal laying forms (positions and sizes) on thermal comfort, respectively.

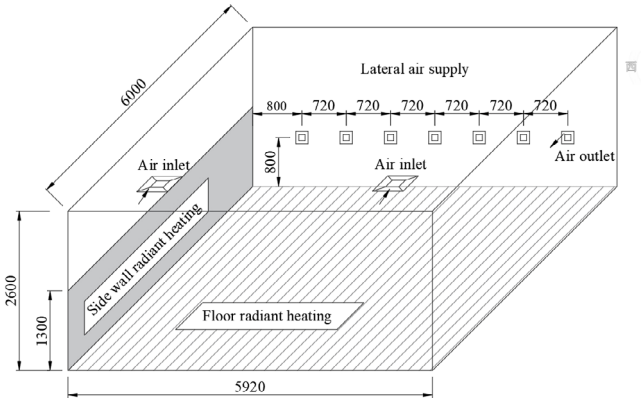

Fig. 6 Schematic diagram of different heating modes

3.2 Grid independence test

The hexahedral unstructured mesh was generated and the maximum mesh size was 0.04 m × 0.04 m × 0.04 m. Five different grid numbers, i.e., 960191, 1125624, 1719493, 2097575, and 2342070 were chosen for the grid independence test, as shown in Table 4. The max error denoted the maximum temperature difference of the 9 points simulated by two adjacent grids. Its value between Cases i and ii was 1.9%, while that for other cases were all less than 1%. However, the monitored CPU time of Case iv/v was about twice/three times of Case iii. Comprehensively considering the simulation accuracy and CPU time, the grid number 1719493 was adopted for subsequent simulations.

3.3 Evaluation indices

The indoor thermal environment for occupants could be evaluated in terms of overall and local thermal comfort (Causone et al. 2010). Hence the overall thermal comfort evaluation indices, including effective draft temperature (EDT), air diffusion performance index (ADPI), predicted mean vote (PMV), predicted percent of dissatisfaction (PPD), and local thermal comfort indices, including local percentage dissatisfied caused by draught, vertical air temperature difference, warm floor and radiant asymmetry (LPD1–LPD4) were evaluated and compared.

3.3.1 Overall thermal comfort evaluation indices

3.3.1.1 EDT

EDT reflected the hot and cold comfort feeling under a

Table 3 Radiation and convection heating parameters

Scenario	Layout	Indoor design temperature (°C)	Heating film temperature (°C)	Air supply temperature (°C)	Ventilation rate (h^{-1})
I	Lateral air supply + adjacent side wall radiation	18	32.42	22.11	4.5
II	Lateral air supply + opposite side wall radiation		32.42	22.11	
III	Lateral air supply + floor radiation		29.29	22.28	
IV	Lateral air supply + adjacent side wall radiation + floor radiation		29.71	18.96	
V	Lateral air supply + opposite side wall radiation + floor radiation		29.71	18.96	

Table 4 Grid independence test result

Case	Grid number	CPU time (min)	Point temperature (°C)									Max error (%)
			1	2	3	4	5	6	7	8	9	
i	960191	15	20.8	21.0	20.4	20.8	21.3	21.2	20.2	21.1	20.8	—
ii	1125624	23	21.0	21.2	20.6	21.0	21.5	21.2	20.6	21.4	21.1	1.9
iii	1719493	34	20.9	21.6	20.9	20.7	21.7	21.3	20.5	21.4	21.0	0.9
iv	2097575	75	20.9	21.6	20.9	20.8	21.6	21.2	20.6	21.5	21.2	0.9
v	2342070	90	21.1	21.6	21.0	20.9	21.6	21.2	20.8	21.5	21.3	0.0

certain air distribution condition. It was defined in Eq. (1) (ISO 2005), and the comfort range distinguished by EDT is shown in Table 5.

$$\mathrm{EDT} = t_i - t_{\mathrm{n}} - 7.66 \times (u_i - 0.15) \quad (1)$$

3.3.1.2 ADPI

ADPI was related with the air temperature, air velocity, and overall thermal comfort, defined as the total number percentage of measuring points in the occupied zone when −1.7 < EDT < +1.1. The higher the ADPI value, the more satisfied of occupants the occupied zone. The formula was given as follows (ISO 2005):

$$\mathrm{ADPI} = \frac{-1.7 < \mathrm{EDT} < 1.1 \text{ number of measurement points}}{\text{Total measurement points}} \times 100\% \quad (2)$$

3.3.1.3 PMV & PPD

PMV index denotes the average index of group voting for seven levels of thermal sensation (from −3 to +3, corresponding to the cold to hot thermal feeling), as shown in Table 6. PPD refers to the dissatisfied percentage of thermal environment, and the evaluation grade index is presented in Table 7. Parameters related to occupants for calculating PMV–PPD indices were set by referring to Fang et al. (2011). Specifications were as follows: clothing value (1.0 clo), external work (1.0 met), metabolic rate (1.0 met), relative humidity (60%), and pressure (101325 Pa). Air velocities and temperatures were obtained with the simulated models.

3.3.2 Local thermal comfort evaluation indices

3.3.2.1 LPD1

LPD1 index was expressed as the percentage to be bothered by draught (ISO 2005). LPD1 < 20% was acceptable for most occupants. The definition of LPD1 was shown as:

$$\mathrm{LPD1} = \left(34 - t_{\mathrm{a}}\right)\left(v - 0.05\right)^{0.62}\left(0.37 v Tu + 3.14\right) \times 100\% \quad (3)$$

$$Tu = \sqrt{v'^2} \,/\, v \quad (4)$$

$$v' = \sqrt{\frac{1}{N-1}\sum_{i=1}^{N}\left(v_i - v\right)^2} \quad (5)$$

3.3.2.2 LPD2

When the air temperature difference between head and ankle height was less than 8 °C, the local dissatisfaction rate should be calculated according to Eq. (6) (ISO 2005):

$$\mathrm{LPD2} = \frac{100}{1 + \exp(5.76 - 0.856\Delta t_{\mathrm{a,y}})} \quad (6)$$

3.3.2.3 LPD3

If the radiant floor was too cool or too warm, occupants might feel dissatisfied due to the thermal sensation of feet. Hence LPD3 was determined as follows (ISO 2005):

$$\mathrm{LPD3} = 100 - 94\exp(-1.387 + 0.118 t_{\mathrm{p}} - 0.0025 t_{\mathrm{p}}^2) \quad (7)$$

3.3.2.4 LPD4

The average radiation temperature (t_{mrt}) was a hypothetical isothermal enclosure surface temperature. The radiant heat exchange between the hypothetical surface and human body was equal to that between human body and surrounding envelope surfaces (ASHRAE 2017). The temperature could be determined by the inner surface temperature and angle coefficient between human body and each envelope surface, as calculated by Eq. (8):

$$t_{\mathrm{mrt}} = \sum_{j=1}^{k}(F_j t_j) \quad (8)$$

Fanger et al. (1980) proposed the asymmetric radiation temperature (Δt_{pr}) to denote the difference of plane radiation temperature between two opposite micro element planes at a certain position. The calculation formulas were shown in Eqs. (9) and (10):

$$t_{\mathrm{pr}} = F_1 t_1 + F_2 t_2 + \cdots + F_N t_N \quad (9)$$

$$\Delta t_{\mathrm{pr}} = t_{\mathrm{pr1}} - t_{\mathrm{pr2}} \quad (10)$$

If the radiant side wall was too cool or too warm, there was an asymmetric thermal radiation field around occupants,

Table 5 Cold and hot comfort range distinguished by EDT

Category	Cold sensation		Thermal neutrality	Thermal sensation	
EDT	EDT < −1.7	−1.7 < EDT < 0	EDT = 0	0 < EDT < 1.1	EDT > 1.1
Feeling	Cold blowing feeling	Comfortable feeling	Thermal neutrality	Hot air feeling	Heat blowing feeling

Table 6 PMV thermal sensation scale

Thermal sensation	Cold	Cool	Slightly cool	Moderate	Slightly warm	Warm	Hot
PMV	−3	−2	−1	0	+1	+2	+3

Table 7 Relationship of PMV and PPD

Grade	PPD	PMV
I	PPD < 10%	−0.5 < PMV < +0.5
II	10% < PPD < 25%	−1 < PMV < −0.5 or +0.5 < PMV < +1
III	PPD > 25%	PMV < −1 or PMV > +1

which might cause local thermal discomfort and reduce acceptability of indoor thermal environment. The difference between the radiant temperature asymmetry was in opposite directions, and it was determined at waist level (0.6 m in height) for a seated occupant (ASHRAE 2011). LPD4 caused by the warm wall when Δt_{pr} < 35 °C was given as follows (ISO 2005):

$$\mathrm{LPD4} = \frac{100}{1+\exp(3.72-0.052\Delta t_{pr})} - 3.5 \quad (11)$$

4 Results and discussion

4.1 Model validations

To verify the model accuracy, horizontal and vertical temperature distributions of Scenario I obtained by experiments and simulations were compared. 9 temperature measurement points with a height of 0.7 m were selected for horizontal comparison, as shown in Figure 7. 11 temperature measuring points at L5 measurement line were selected for vertical comparison, as shown in Table 8.

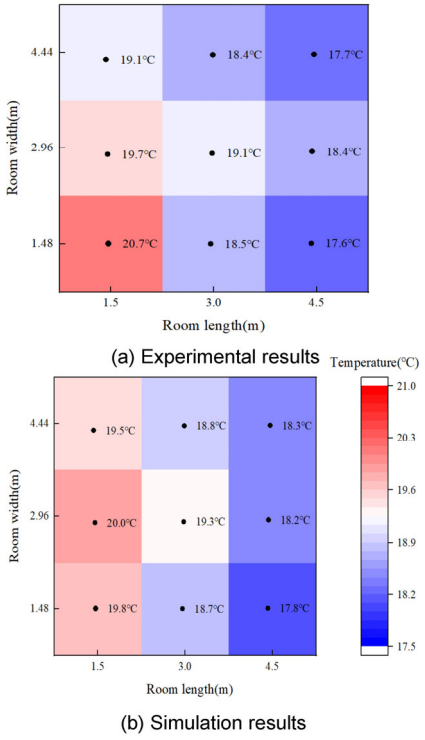

Fig. 7 Temperature validation at horizontal direction

Table 8 Temperature validation at vertical direction

Height (m)	Experimental value (°C)	Numerical value (°C)	Absolute error (°C)
0.1	18.8	19.2	0.3
0.3	18.3	19.2	0.9
0.5	18.8	19.3	0.5
0.7	19.1	19.3	0.2
0.9	19.2	19.4	0.2
1.1	18.8	19.4	0.6
1.3	18.9	19.5	0.6
1.5	19.0	19.5	0.5
1.7	19.0	19.5	0.5
1.9	19.0	19.5	0.5
2.4	18.9	19.3	0.4

The experimental temperatures in horizontal and vertical directions were generally lower than the simulation values, which might be caused by the instrument error and accidental cold air penetration in the experimental cabin. Nevertheless, the average numerical temperature at the horizontal direction was 0.1 °C higher than the experimental one, and the maximum temperature difference was −0.9 °C. And the average numerical temperature at the vertical direction was 0.5 °C higher than the experimental one, and the maximum temperature difference was 0.9 °C. The numerical results were regarded as reliable and applicable.

4.2 Asymmetric radiation temperature

The wall and asymmetric radiation temperature were summarized in Table 9 to compare the asymmetry of five scenarios. The asymmetric radiation temperatures in the horizontal direction of different scenarios were relatively close, and their absolute values were lower than vertical ones. The vertical asymmetric radiation temperatures of Scenarios I and II were −7.0 and −5.4 °C respectively, and that of Scenario III, IV, and V were −13.3, −12.7, and −12.1 °C, respectively. The phenomenon was mainly caused by the following two reasons. The temperature difference between the ceiling and floor under Scenario I and II were both 3.8 °C, and that under Scenario III, IV and V were 13.7–14.3 °C. The angle coefficient of side wall radiation system was 0.18, while that of the floor radiation system was 0.39. The greater the floor radiation angle coefficient, the higher the average temperature of lower micro element surface, and the greater the temperature difference between the upper and lower micro element surfaces.

4.3 Effect of different heating modes

To investigate the combination effect of different heating

modes, the following three scenarios were simulated and compared, i.e., (I) lateral air supply + adjacent side wall radiation, (III) lateral air supply + floor radiation, and (IV) lateral air supply + adjacent side wall radiation + floor radiation.

4.3.1 *Overall thermal comfort*

Temperature and velocity contour at X = 3 m section for Scenarios I, II, and III are depicted in Figure 8. In Scenario I, the heating film was located on the side wall, leading to the maximum air temperature difference near the radiant wall and exterior window with a value of 5.2 °C. Scenario III had a more uniform temperature distribution, and its maximum air temperature difference was 2.1 °C. While in Scenario IV, hot air was directly blown to the radiation side wall, resulting in a 1 °C lower of temperature difference than Scenario I. As a result, the temperature distribution of the occupied area in Scenario III was described as the most uniform.

The PMV, PPD, and ADPI indices at head height (Y = 1.1 m) in sitting posture were compared, as presented in Figs. 9 and 10. In Scenario I, the heating film was located on the south wall, so PMV increased by 0.4 and PPD decreased by 19.5% from the north wall to south wall. In Scenario III, the radiant floor was utilized, the temperature of surrounding walls was lower, and the PMV value at the room center was higher than that of the surrounding. Compared with Scenario I, the PMV and PPD of Scenario III increased by 0.15 and decreased by 1.52%, respectively. In Scenario IV, the overall thermal comfort was improved for the increasing radiation area and radiation angle coefficient. The PMV and PPD difference from the south wall to north wall decreased to 0.3 and 10.8%, respectively.

The average PMV, PPD, and ADPI for Scenario I were −1.6, 56.6%, and 26.2%, which increased by 0.6/0.6, −25.9%/−26.5%, 7.2%/22.5% respectively for Scenario III/IV. Compared with Scenario I, the radiation area and radiation angle coefficient of Scenario III/IV were larger, wherefore the thermal comfort of the occupied area was enhanced.

4.3.2 *Local thermal comfort*

Temperature contours at the height of Y = 0.1 and 1.1 m are depicted in Figure 11. Temperature values of 9 points evenly distributed in the occupied area were selected to analyze the vertical temperature difference, and the results are presented in Figure 12. The average temperature at Y = 0.1 m for Scenarios I, III, and IV were 19.0, 21.7, and 20.5 °C, respectively, and at Y = 1.1 m were 19.3, 21.1, and 20.2 °C, respectively, resulting in the vertical temperature differences

Table 9 Summary of wall and asymmetric radiation temperature

Scenario	Wall temperature (°C)								Asymmetric radiation temperature (°C)	
	East	West	South	North	Floor	Ceiling	Window	ERHP	Vertical	Horizontal
I	15.4	12.6	14.6	10.8	19.2	15.4	7.3	32.4	−7.0	4.2
II	16.6	12.7	16.6	11.2	19.2	15.4	7.8	32.4	−5.4	2.7
III	17.9	15.9	15.7	13.0	29.3	15.6	9.1	29.3	−13.3	1.6
IV	17.9	14.0	15.2	12.6	29.8	15.5	9.4	29.4	−12.7	4.4
V	17.3	13.9	15.4	12.9	29.8	15.6	9.6	29.4	−12.1	2.4

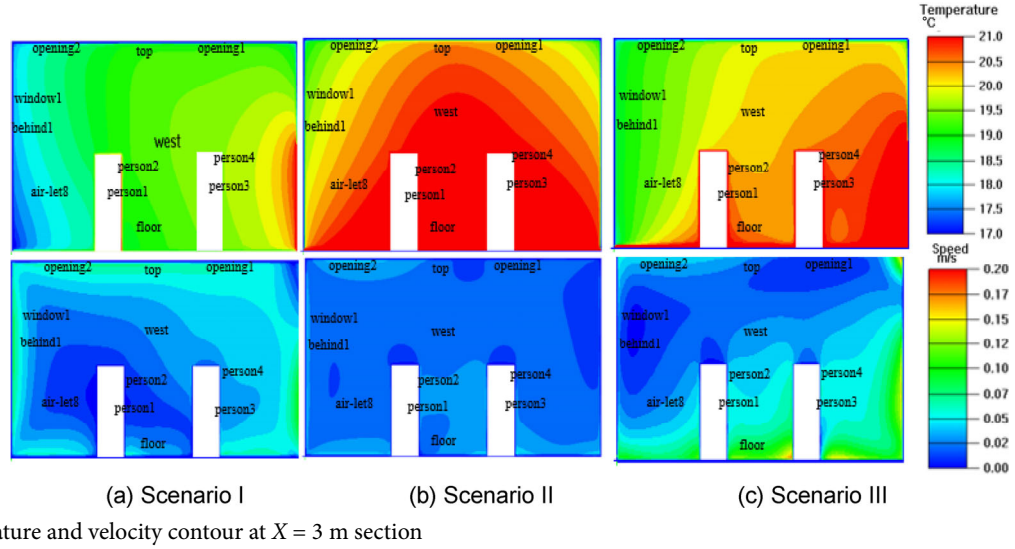

Fig. 8 Temperature and velocity contour at X = 3 m section

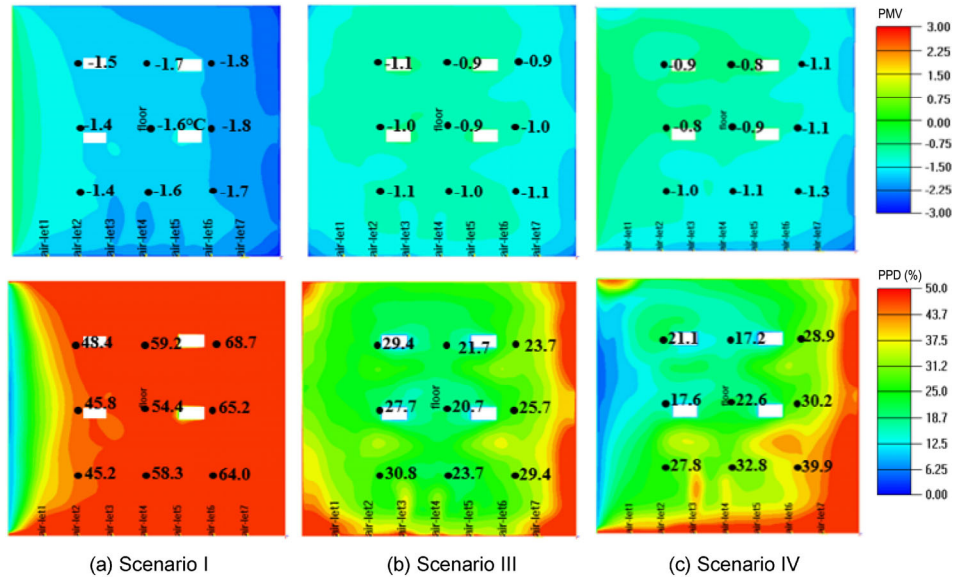

Fig. 9 PMV and PPD contour at Y = 1.1 m section

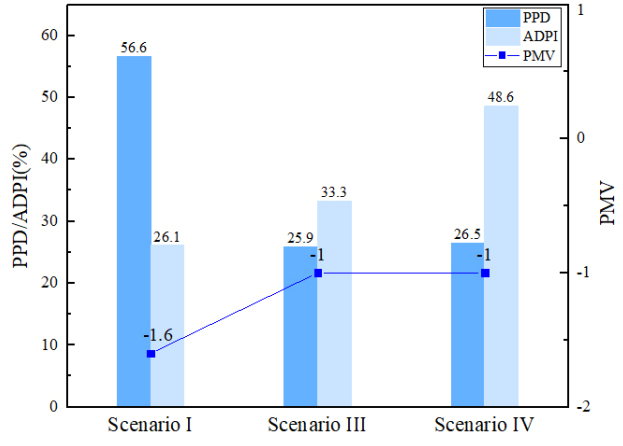

Fig. 10 Comparison of overall thermal comfort indices

of 0.3, 0.6, and 0.3 °C, respectively. The vertical temperature differences could meet the requirement of ISO-7730 Standard (ISO 2005), of which the temperature difference between Y = 0.1 and 1.1 m in height was required to be not more than 3 °C. In the form of floor heating + displacement ventilation, Causone et al. (2010) found the average vertical temperature difference was 1.1 °C, which was higher than the value of 0.5–0.8 °C in this study. Therefore local comfort was improved under Scenarios I, III, and IV.

The local thermal comfort calculation results of these three scenarios are shown in Table 10. Causone et al. (2010) obtained that LPD1 of floor radiation + displacement ventilation was 8%, while LPD1 of Scenario I/II/III in the present study was 11.0%/9.0%/8.0%. When LPD1 was less

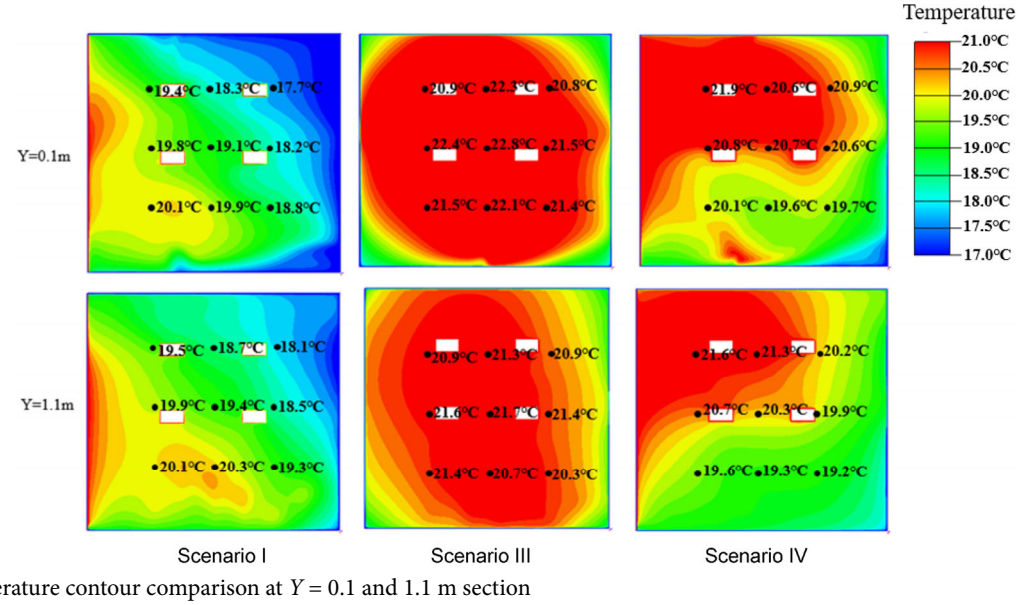

Fig. 11 Temperature contour comparison at Y = 0.1 and 1.1 m section

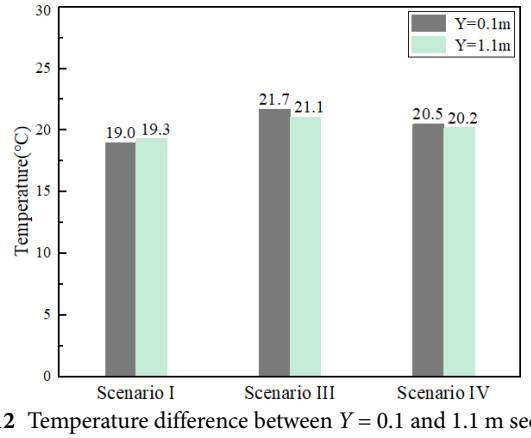

Fig. 12 Temperature difference between $Y = 0.1$ and 1.1 m section

Table 10 Local evaluation indices of different heating modes

Scenario	LPD1	LPD2	LPD3	LPD4
(I) Adjacent side wall + air supply	11.2%	0.4%	22.2%	8.1%
(III) Floor + air supply	9.0%	0.1%	12.8%	6.5%
(IV) Floor + adjacent side wall + air supply	8.0%	0.2%	14.1%	6.7%

than 10%, buildings belonged to "A" class according to the ISO-7730 Standard. While LPD1 of Scenario I was higher than 10%, due to the small radiation area of side wall and high temperature of local heat source. In addition, LPD2 of the three scenarios were all less than 1%, which is less than 5%. Thus under limitations for buildings in Category A (ISO 2005), which indicates that the vertical temperature difference is not obvious. LPD3/LPD4 of Scenario I was 22.2%/8.1%, which was 9.4%/1.6% and 8.1%/1.4% higher than those of Scenarios III and IV, respectively. This was because the radiation area and radiation angle coefficient to human body in Scenario I were relatively small, so the overall heat dissipation performance and heat directly radiated to human body were less, inducing more local discomfort sensation. While the local thermal comfort differences in Scenarios III and IV were slight, indicating the local thermal comfort indices did not rise significantly with the increase of radiation area.

4.4 Effect of different heating terminal positions

To investigate the effect of different heating terminal positions, the following four scenarios were simulated and compared, i.e., (I) lateral air supply + adjacent side wall radiation, (II) lateral air supply + opposite side wall radiation, (IV) lateral air supply + adjacent side wall radiation + floor radiation, and (V) lateral air supply + opposite side wall radiation + floor radiation.

4.4.1 Overall thermal comfort

The temperature and velocity distribution were more uniform when the heating film was arranged opposite to air supply outlets than adjacent to air supply outlets, as shown in Figure 13. Compared with Scenarios I and II, the average indoor temperature and wind speed of Scenarios IV and V increase by about 1.8 °C and 0.04 m/s, respectively. The addition of heating film area increased the indoor temperature and the rise of warm air accelerated the airflow. But no matter the air supply outlets were adjacent or opposite to the side wall heating film, the thermal comfort of lateral air supply + side wall radiation + floor radiation was better. The area of the heating film had a greater impact on improving the indoor environment than the relative position of the heating film and the air supply outlets.

The PMV, PPD, and ADPI indices at head height (Y = 1.1 m) in sitting posture were compared, as presented in Figs. 14 and 15. As depicted in the figures, the PMV, PPD, and ADPI of Scenario I/II were −1.6/−1.6, 56.6%/57.3%, and

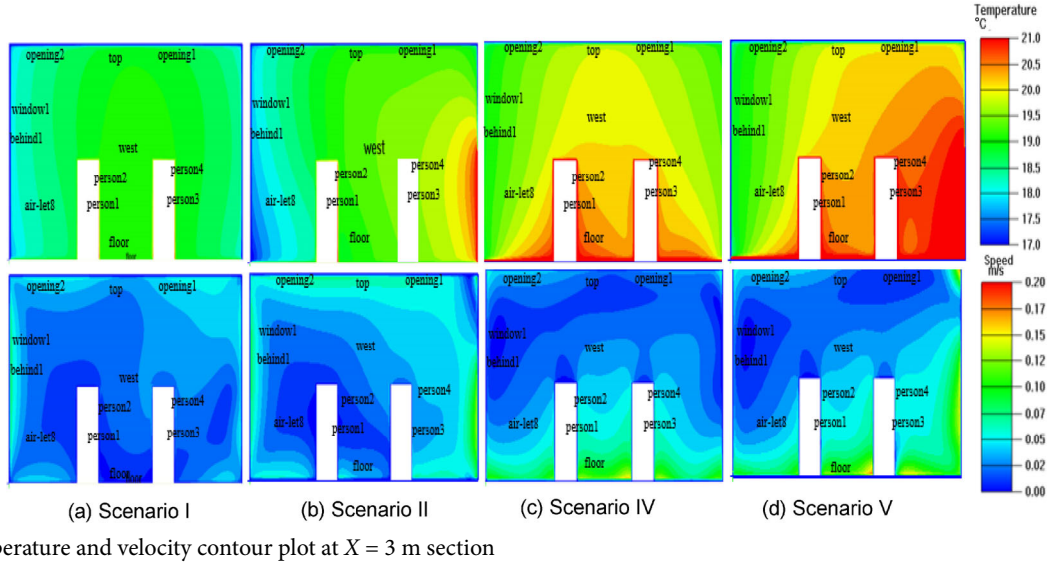

Fig. 13 Temperature and velocity contour plot at $X = 3$ m section

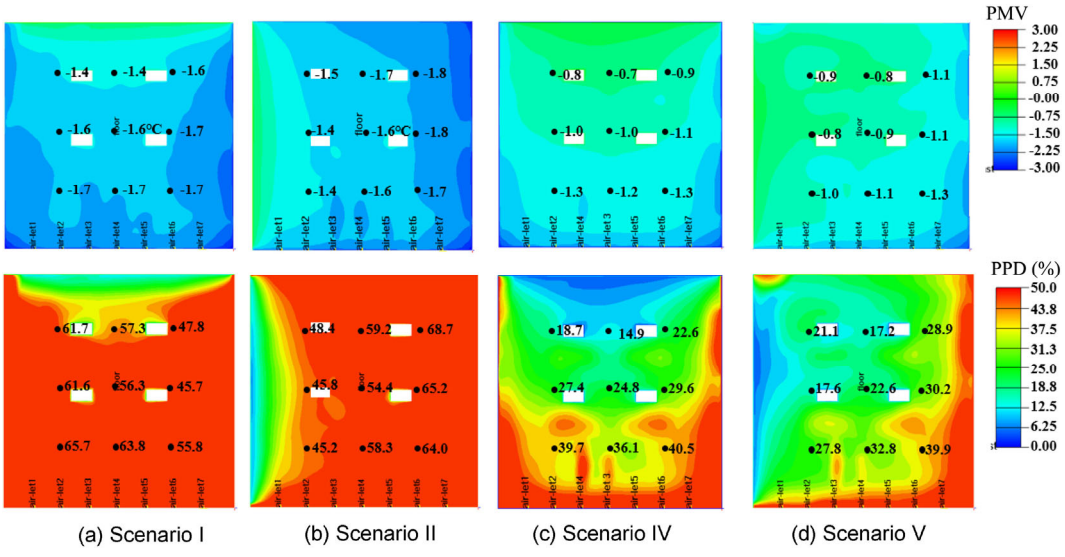

Fig. 14 PMV and PPD contour with different heating terminal positions

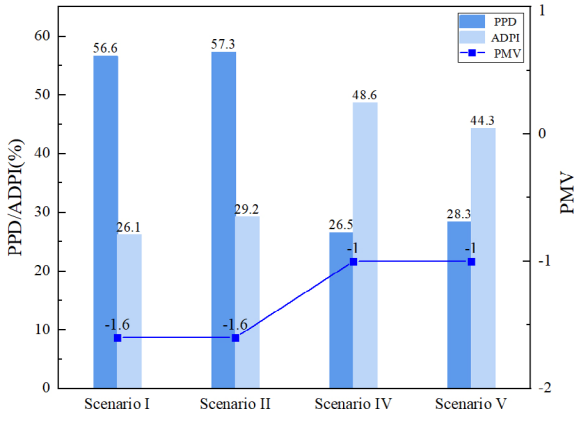

Fig. 15 Overall thermal comfort indices with different heating terminal positions

26.2%/29.2%, respectively. When the heating film and air outlets changed from adjacent position to relative position, PPD and ADPI decreased by 3.1% and 0.7%, respectively. The PMV, PPD, and ADPI of Scenario IV/V were −1/−1, 26.5%/28.3%, and 48.6%/44.3%, respectively. When the heating film and air supply outlets changed from adjacent position to opposite position, PPD and ADPI increased by 4.3% and 1.8%, respectively. At the opposite position, the convective heat transfer rate of heating film to the indoor air was enhanced, resulting in more heat transferred to the occupied area. Moreover, the overall thermal comfort of Scenario IV/V were superior to that of Scenario I/II, demonstrating the radiation area was a main factor in thermal environment regulation.

4.4.2 *Local thermal comfort*

As shown in Figs. 16 and 17, the average temperature at Y = 0.1 m of Scenarios I, II, IV, and V were 19.0, 19.0, 20.7, and 20.5 °C, respectively, and at Y = 1.1 m were 19.2, 19.3,

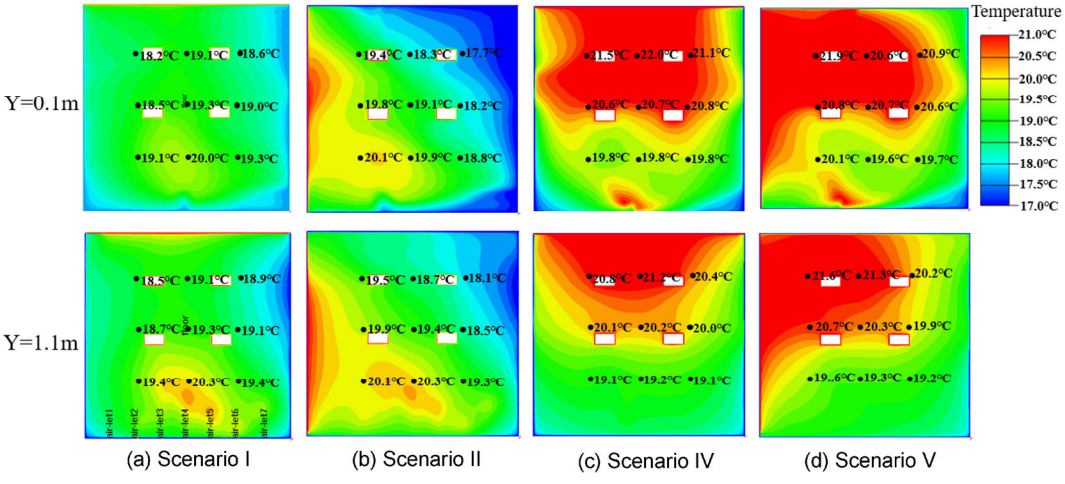

Fig. 16 Temperature contour at Y = 0.1 and 1.1 m section with different heating terminal positions

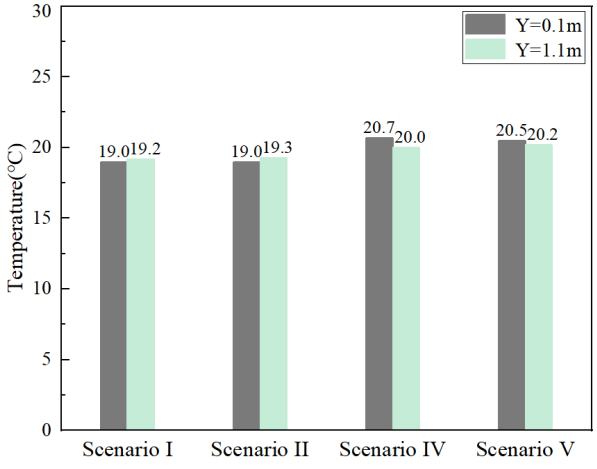

Fig. 17 Temperature difference between Y = 0.1 and 1.1 m section with different heating terminal positions

20.0, and 20.2 °C, respectively. Accordingly, the average vertical air temperature difference of 0.1 and 1.1 m in height for Scenarios I, II, IV, and V were 0.2, 0.3, 0.7, and 0.3 °C, respectively. Although the vertical air temperature of Scenario IV was relatively higher, it could meet the requirement of ISO-7730 Standard.

5 Conclusions

Aiming at improving the indoor thermal environment in winter, this study investigated the influence of different heating modes (Scenario I, Scenario III, Scenario IV) and different heating positions (Scenario I, Scenario II, Scenario IV, Scenario V) on occupants overall thermal comfort (EDT, ADPI, PMV, and PPD) and local thermal comfort (LPD1–LPD4). The main arising findings were as follows:

(i) The relative position of side wall heating film and air outlet were shown to have little effect on overall thermal comfort. The PMV, PPD, and ADPI of Scenario I/II were −1.6/−1.6, 57.3%/56.6%, and 29.2%/26.2%, respectively. Those of Scenario III/IV/V were −1/−1/−1, 25.9%/28.3%/26.5%, and 33.3%/44.3%/48.6%, respectively. The overall thermal comfort of Scenario III/IV/V was better than Scenario I/II, indicating that the radiation area was the main factor in thermal environment regulation.

(ii) The larger the temperature difference between ceiling and floor, the higher the vertical asymmetric radiation temperature. And the greater the floor radiation angle coefficient, the higher the average temperature of lower micro element surface, the greater the temperature difference between the upper and lower micro element surfaces. As a result, the vertical asymmetric radiation temperature of Scenario I/II was about 6.5 °C lower than that of Scenario III/IV/V.

(iii) For Scenarios I–III, the local dissatisfaction rates caused by vertical air temperature difference (LPD2) were 0.4%, 0.1%, and 0.2%, respectively, which belonged to "A" class according to the ISO-7730 Standard. The LPD3/LPD4 of Scenario I was 22.2%/8.1%, which were 9.4%/1.6% and 8.1%/1.4% higher than those of Scenarios III and IV, respectively. The coupling mode of Scenarios III and IV improved the local discomfort by increasing radiation area and radiation angle coefficient to human body.

This study provided methods for the optimal design and control of indoor thermal environment with aspect of overall and local thermal comfort. In the near future, more heating modes and terminal laying forms needed to be investigated, and the energy consumption and cost-effectiveness were required to be comprehensively considered.

Acknowledgements

This study was financially supported by the National Natural Science Foundation of China (No. 51978231), the Opening Funds of State Key Laboratory of Building Safety and Built Environment and National Engineering Research Center of Building Technology (No. BSBE2019-02), S&T Program of Hebei (No. 216Z4502G), the Natural Science Foundation of Hebei Province (No. E2020202196), the Fundamental Research Funds of Hebei University of Technology (No. JBKYTD2003), and Hebei Province Funding Project for Returned Scholars, China (No. C20190507).

References

Alonso MJ, Andresen T, Frydenlund F, et al. (2011). Improvements of air flow distribution in a freezing tunnel using Airpak. *Procedia Food Science*, 1: 1231–1238.

ASHRAE (2011). ANSI/ASHRAE Standard 55-2010: Thermal Environment Conditions for Human Occupancy. Atlanta, GA, USA: American Society of Heating, Ventilating and Air-Conditioning Engineers.

ASHRAE (2017). ASHRAE Handbook Fundamentals. Atlanta, GA, USA: American Society of Heating, Refrigeration and Air-Conditioning Engineers.

ASHRAE (2020). ASHRAE Position Document on Infectious Aerosols. Atlanta, GA, USA: American Society of Heating, Refrigeration and Air-Conditioning Engineers.

Atienza Márquez A, Cejudo López JM, Fernández Hernández F, et al. (2017). A comparison of heating terminal units: Fan-coil versus radiant floor, and the combination of both. *Energy and Buildings*, 138: 621–629.

Bäckström D, Johansson R, Andersson K, et al. (2015). On the use of alternative fuels in rotary kiln burners—An experimental and modelling study of the effect on the radiative heat transfer conditions. *Fuel Processing Technology*, 138: 210–220.

Camci M, Karakoyun Y, Acikgoz O, et al. (2021). A comparative study on convective heat transfer in indoor applications. *Energy and Buildings*, 242: 110985.

Causone F, Baldin F, Olesen BW, et al. (2010). Floor heating and cooling combined with displacement ventilation: Possibilities and limitations. *Energy and Buildings*, 42: 2338–2352.

Conceição EZE, Lúcio MMJR (2011). Evaluation of thermal comfort conditions in a classroom equipped with radiant cooling systems and subjected to uniform convective environment. *Applied Mathematical Modelling*, 35: 1292–1305.

Dai H, Zhao B (2020). Association of the infection probability of COVID-19 with ventilation rates in confined spaces. *Building Simulation*, 13: 1321–1327.

Dong J, Zhang L, Deng S, et al. (2018). An experimental study on a novel radiant-convective heating system based on air source heat pump. *Energy and Buildings*, 158: 812–821.

Energy Conservation Research Center of Tsinghua University (2020). Annual report on China building energy efficiency 2020: Special topic on rural housing. Beijing: China Architecture and Building Press.

Fang T, Hang F, Wu B (2011). Indoor ventilation simulation in green building based on Airpak. In: Proceedings of the International Conference on Computer Distributed Control and Intelligent Environmental Monitoring, Changsha, China.

Fanger PO, Ba'nhidi L, Olesen BW, et al. (1980). Comfort limits for heated ceilings. *ASHRAE Transactions*, 86(2): 141–156.

Hu J (2015). Analysis of heat balance in ground source heat pump system and its application in large scale public buildings. *Chinese Journal of Refrigeration Technology*, 35(02): 63–67.

ISO (2005). ISO 7730:2005. Ergonomics of the Thermal Environment—Analytical Determination and Interpretation of Thermal Comfort Using Calculation of the PMV and PPD Indices and Local Thermal Comfort Criteria. Geneva: International Organization for Standardization.

Ji W, Chen C, Zhao B (2021). A comparative study of the effects of ventilation-purification strategies on air quality and energy consumption in Beijing, China. *Building Simulation*, 14: 813–825.

Kong X, Guo C, Lin Z, et al. (2021). Experimental study on the control effect of different ventilation systems on fine particles in a simulated hospital ward. *Sustainable Cities and Society*, 73: 103102.

Lin Z, Wang J, Yao T, et al. (2012). Investigation into anti-airborne infection performance of stratum ventilation. *Building Simulation,* 54: 29–38.

Liu J, Dalgo DA, Zhu S, et al. (2019). Performance analysis of a ductless personalized ventilation combined with radiant floor cooling system and displacement ventilation. *Building Simulation,* 12: 905–919.

Ploskić A, Holmberg S (2011). Low-temperature baseboard heaters with integrated air supply—An analytical and numerical investigation. *Building and Environment*, 46: 176–186.

Qian H, Miao T, Liu L, et al. (2021). Indoor transmission of SARS-CoV-2. *Indoor Air*, 31: 639–645.

Ren C, Cao S (2021). Construction of linear temperature model using non-dimensional heat exchange ratio: Towards fast prediction of indoor temperature and heating, ventilation and air conditioning systems control. *Energy and Buildings*, 251: 111351.

Rhee KN, Kim KW (2015). A 50 year review of basic and applied research in radiant heating and cooling systems for the built environment. *Building and Environment*, 91: 166–190.

Schiavon S, Bauman FS, Tully B, et al. (2015). Chilled ceiling and displacement ventilation system: Laboratory study with high cooling load. *Science and Technology for the Built Environment*, 21: 944–956.

Seyam S, Huzayyin A, El-Batsh H, et al. (2014). Experimental and numerical investigation of the radiant panel heating system using scale room model. *Energy and Buildings*, 82: 130–141.

Sui X, Tian Z, Liu H, et al. (2021). Field measurements on indoor air quality of a residential building in Xi'an under different ventilation modes in winter. *Journal of Building Engineering*, 42: 103040.

Tian Z, Wang S, Zhu N, et al. (2010). Performance and thermal comfort of chilled ceiling system in heating mode. *Journal of Tianjin University*, 43(12): 1109–1114. (in Chinese)

Wang Z, He Y, Hou J, et al. (2013). Human skin temperature and thermal responses in asymmetrical cold radiation environments. *Building and Environment*, 67: 217–223.

Wang D, Wu C, Liu Y, et al. (2017). Experimental study on the thermal performance of an enhanced-convection overhead radiant floor heating system. *Energy and Buildings*, 135: 233–243.

Wang H, Qian H, Zhou R, et al. (2020). A novel circulated air curtain system to confine the transmission of exhaled contaminants: A numerical and experimental investigation. *Building Simulation*, 13: 1425–1437.

Xu C, Luo X, Yu C, et al. (2020). The 2019-nCoV epidemic control strategies and future challenges of building healthy smart cities. *Indoor and Built Environment*, 29: 639–644.

Zhang D, Cai N, Wang Z (2013). Experimental and numerical analysis of lightweight radiant floor heating system. *Energy and Buildings*, 61: 260–266.

Zhang L, Dong J, Jiang Y, et al. (2018). An experimental study on frosting and defrosting performances of a novel air source heat pump unit with a radiant-convective heating terminal. *Energy and Buildings*, 163: 10–21.

Zhang S, Lin Z, Ai Z, et al. (2019). Effects of operation parameters on performances of stratum ventilation for heating mode. *Building and Environment*, 148: 55–66.

Zhang J, Zhou X, Lei S, et al. (2021). Energy and comfort performance of occupant-centric air conditioning strategy in office buildings with personal comfort devices. *Building Simulation,* https://doi.org/10.1007/s12273-021-0852-1.

Zhao Q, Lian Z, Lai D (2021). Thermal comfort models and their developments: A review. *Energy and Built Environment*, 2: 21–33.

Zhu X, Shi T, Jin X, et al. (2021). Multi-sensor information fusion based control for VAV systems using thermal comfort constraints. *Building Simulation,* 14: 1047–1062.